

Connective Tissue Characteristics around Healing Abutments of Different Geometries: New Methodological Technique under Circularly Polarized Light

Rafael Arcesio Delgado-Ruiz, DDs, MSc, PhD;* Jose Luis Calvo-Guirado, DDs, MSc, PhD;†
Marcus Abboud, MD, MSc, PhD;‡ Maria Piedad Ramirez-Fernandez, DDs, MSc, PhD;§
José Eduardo Maté-Sánchez de Val, DDs, MSc, PhD;¶ Bruno Negri, DDs, MSc, PhD;**
Gerardo Gomez-Moreno, DDs, PhD;†† Aleksa Markovic, DDs, PhD‡‡

ABSTRACT

Purpose: To describe contact, thickness, density, and orientation of connective tissue fibers around healing abutments of different geometries by means of a new method using coordinates.

Materials and Methods: Following the bilateral extraction of mandibular premolars (P2, P3, and P4) from six fox hound dogs and a 2-month healing period, 36 titanium implants were inserted, onto which two groups of healing abutments of different geometry were screwed: Group A (concave abutments) and Group B (wider healing abutment). After 3 months the animals were sacrificed and samples extracted containing each implant and surrounding soft and hard tissues. Histological analysis was performed without decalcifying the samples by means of circularly polarized light under optical microscope and a system of vertical and horizontal coordinates across all the connective tissue in an area delimited by the implant/abutment, epithelium, and bone tissue.

Results: In no case had the connective tissue formed a connection to the healing abutment/implant in the internal zone; a space of $35 \pm 10 \mu\text{m}$ separated the connective tissue fibers from the healing abutment surface. The total thickness of connective tissue in the horizontal direction was significantly greater in the medial zone in Group B than in Group A ($p < .05$). The orientation of the fibers varied according to the coordinate area so that internal coordinates showed a higher percentage of parallel fibers in Group A ($p < .05$) and a higher percentage of oblique fibers in Group B ($p < .05$); medial coordinates showed more oblique fibers ($p < .05$); and the area of external coordinates showed the highest percentage of perpendicular fibers ($p < .05$). The fiber density was higher in the basal and medial areas ($p < .05$).

Conclusions: Abutment geometry influences the orientation of collagen fibers; therefore, an abutment with a profile wider than the implant platform favors oblique and perpendicular orientation of collagen fibers and greater connective tissue thickness.

KEY WORDS: connective tissue, dental implants, healing abutments, histology, polarized light

*Assistant professor, Department of Prosthodontics and Digital Technology, School of Dental Medicine, Stony Brook University, Stony Brook, NY, USA; †associate professor and chairman of Department of Implant Dentistry, Faculty of Medicine and Dentistry, Murcia University, Murcia, Spain; ‡associate professor and chairman of Department of Prosthodontics and Digital Technology, School of Dental Medicine, Stony Brook University, Stony Brook, NY, USA; §assistant professor, Department of Implant Dentistry, Faculty of Medicine and Dentistry, Murcia University, Murcia, Spain; ¶associate professor, Department of Restorative Dentistry, Faculty of Medicine and Dentistry, Murcia University, Alicante, Alicante, Spain; **visiting professor, Department of Implant Dentistry, Faculty of Medicine and Dentistry, Murcia University, Pilar de la Horadada, Alicante, Spain;

††associate professor and chairman of Department of Special Care and Pharmacological Research in Dentistry, Faculty of Medicine and Dentistry, Granada University, Granada, Spain; ‡‡professor and chairman of Clinic of Oral Surgery, Faculty of Stomatology, University of Belgrade, Belgrade, Serbia

Reprint requests: Assistant Professor Rafael Arcesio Delgado-Ruiz, DDs, MSc, PhD, Department of Prosthodontics and Digital Technology, School of Dental Medicine, Stony Brook University, Stony Brook, 1104 Westchester Hall, Stony Brook, NY 11794-7812, USA; e-mail: Rafael.Delgado-Ruiz@stonybrookmedicine.edu

© 2013 Wiley Periodicals, Inc.

DOI 10.1111/cid.12161

BACKGROUND

Maintaining the integration of dental implants depends (among other factors) on the extent of bone contact and the condition of the peri-implant soft tissues. These tissues have similar characteristics to dentogingival tissues and are made up of epithelium and connective tissue.^{1,2} The components and dimensions of peri-implant soft tissues around implants are similar to those that support natural teeth, except for the shape that the connective tissue adopts in relation to the implant surface.³⁻⁶

In natural dentition, collagen fibers of the periodontal ligament are arranged radially and inserted into the cement of the tooth's cervical area, which maximizes resistance to tension forces.⁷ With implants, while longitudinal and circumferential fibers whose axes are parallel or oblique establish themselves in the cervical area of titanium implants; this takes place without direct insertion of the connective tissue into the implant surface.⁸⁻¹⁰

Soft tissues also play their part in protecting and maintaining the integrity of the peri-implant bone; in the crestal area they prevent bacterial invasion by means of different mechanisms in each of their components,¹¹ provide resistance to frictional forces arising from mastication, and limit the penetration of foreign bodies.¹²⁻¹⁴

Schupbach and Glauser describe four defense zones – sulcular epithelium, junctional epithelium, lamina propria, and gingival tissue fibers – each of which has a specific function; the authors comment that an orientation of the fibers perpendicular to the surface of the implant will prevent the apical migration of junctional epithelium.¹⁵

Although there is some controversy regarding the orientation of connective tissue fibers close to the implant surface, it has been shown that microscopic irregularities,¹⁶ such as those generated by acid etching, or porous surfaces³ could promote the presence of perpendicular fibers.

Another factor that can affect fiber orientation is the presence of keratinized tissue, which favors parallel fibers.¹⁷ Recently, other factors that might favor the presence of perpendicular fibers have been investigated, such as microgrooves of 8 to 12 μm , which permit adherence and fibroblast growth and the direct adherence of collagen fibers in the treated area.¹⁸⁻²⁰ Similarly, the presence of an area of pits of $70 \pm 5 \mu\text{m}$ diameter has also been seen to favor fibroblast adherence and perpendicular connective fibers in a dog model.²¹

For titanium implants inserted crestally without bone loss, the establishment of biologic width can be observed in the transmucosal zone of implants or in the healing or prosthetic abutments. For this reason, modifications have recently been made to the abutment surface with the aim of attempting to achieve the insertion of connective tissue and avoid the apical migration of junctional epithelium.²²⁻²⁵

In a clinical pilot study, Rompen and colleagues²² proposed the use of a type of abutment with a concave surface in the esthetic zone, which would increase soft tissue stability. However, in a clinical study in humans, Palti and colleagues²³ used similar titanium abutments with a concave basal area of 0.5 mm depth by 1.25 mm width, comparing these with conventional abutments and showing that this concavity did not increase marginal tissue stability or resistance to removal.²⁴

The healing abutment material can also affect soft tissue healing; titanium and zirconia have shown good integration, while gold/platinum has shown an increase in inflammatory tissue and absence of soft tissue integration.²⁵ The rapidly evolving development of surfaces, materials, and designs means that each new innovation calls for a reevaluation of implant interfaces and their behavior.²⁶

To date, as far as the authors of this study are aware, the influence of healing abutment geometry on supracrestal connective tissue has not been researched.

The purpose of this study was to describe and quantify the contact and thickness, fiber orientation, and fiber density of connective tissue in two different healing abutment configurations by means of histological study using circularly polarized light and a novel system of vertical and horizontal coordinates.

MATERIALS AND METHODS

Six fox hound dogs of approximately 1 year of age, each weighing 14 to 15 kg, were used in the experiment. The Ethics Committee for Animal Research at the University of Murcia, Spain approved the study (Murcia, July 2011), which followed guidelines established by the European Union Council Directive of November 24, 1986 (86/609/EEC).

Surgical Procedure

The animals were preanesthetized with acepromazine (0.2–1.5 mg/kg) 10 minutes before administration of butorphanol (0.2 mg/kg) and medetomidine (7 mg/kg).

The mixture was injected intramuscularly in the femoral quadriceps. An intravenous catheter was inserted in the cephalic vein and propofol was infused at a slow, constant rate of 0.4 mg/kg/min. These procedures were carried out under the supervision of a veterinary surgeon.

Local infiltrative anesthesia was administered at the surgical sites. An intrasulcular incision was performed from distal of P1 to a point mesial of M1, raising a full-thickness flap to expose the bone crests and entire dental crowns of P2, P3 and P4; the teeth were sectioned in buccolingual direction at the bifurcation using a tungsten carbide bur and the roots extracted individually using a periosteal elevator and forceps, without damaging the bony walls.

Bilateral mandibular tooth extractions (P2, P3, P4) were performed. Wound closure was carried out using single dissolvable sutures (Dexon 3-0, Davis & Geck, American Cyanamid Co., Wayne, NJ, USA).

During the first week after surgery, the animals received antibiotics and analgesics – amoxicillin (500 mg, twice daily) and ibuprofen (600 mg, three times a day) via the systemic route. The dogs were fed a soft diet for 14 days; after that, a normal pellet diet was established.

Implants were placed after a 2-month healing period. After crestal incision, a full-thickness flap at the previous location was reflected, and each site was prepared following the protocol recommended by the implant manufacturer (Bredent Medical® GmbH & Co. KG, Senden, Germany), preparing a bed of 4 mm diameter and 10 mm length. Each hemimandible received three cylindrical screw implants, all with the same dimensions at the intraosseous portion.

Implants and Abutments

Thirty-six commercially manufactured titanium Blue-sky® implants (Bredent Medical) of 4 mm diameter and

10 mm length were inserted at a torque of ≥ 35 Ncm. The implants were placed with their platforms level with the osseous crest. Healing abutments of 2 mm length and of similar surface roughness (R_a $0.3 \mu\text{m} \pm 0.1 \mu\text{m}$) were screwed onto each implant. These had two different geometries. Group A consisted of 18 concave healing abutments (REF SKY-GF02, Bredent Medical), Group B of 18 wide profile healing abutments (REF SKYEMG02, Bredent Medical) (Figure 1).

The abutments were screwed and tightened with a torque of 25 Ncm to prevent loosening, as recommended by the manufacturer. Mucoperiosteal flaps underwent tension-free closure and were sutured with single dissolvable sutures (Dexon 3-0, Davis & Geck, American Cyanamid).

During the first week after surgery, the animals received antibiotics and analgesics – amoxicillin (500 mg, twice daily) and ibuprofen (600 mg, three times a day) via the systemic route. The dogs were fed a soft diet for 14 days; after that, a normal pellet diet was established. For 14 days post-surgery, the oral cavities were rinsed daily with 0.12% chlorhexidine digluconate (Cariax Gingival® mouth rinse, Kin® Laboratories, Barcelona, Spain). During the entire study period, a strict plaque control program was performed daily using a medium toothbrush and 0.2% chlorhexidine gel (Perio Kin® Gel, Kin Laboratories, Barcelona, Spain), as described by Comut and colleagues.¹⁷

Animal Sacrifice

After 3 months, the dogs were sacrificed as follows: the animals were preanesthetized following the protocol described earlier, followed by a perfusion of sodium pentothal (Abbot Laboratories, Chicago, IL, USA) through the carotid artery, supervised by the veterinary

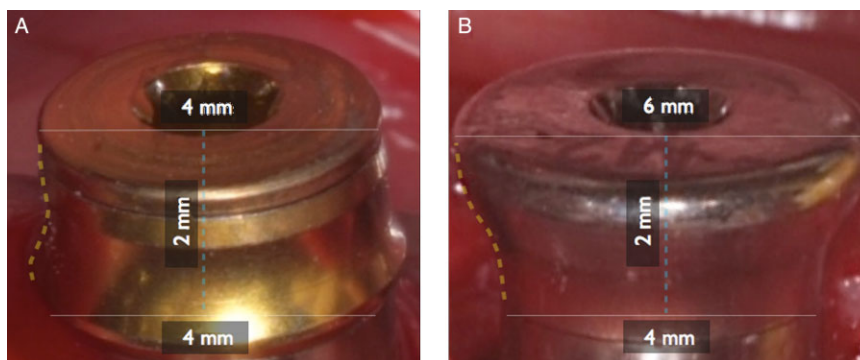


Figure 1 Comparison of healing abutments. Group A: Concave abutment, gold-colored to distinguish between groups. Group B: Wider abutment, gray-colored to distinguish between groups. White lines show the basal and coronal diameters of the abutments; yellow lines show the abutment profile; blue dotted line shows abutment height.

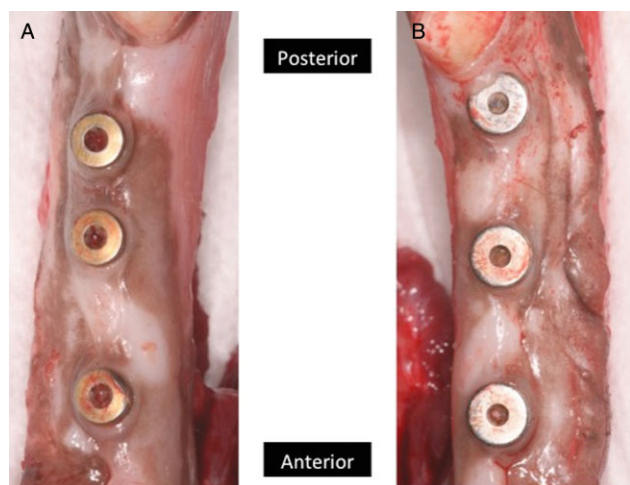


Figure 2 Clinical appearance of jaw blocks at sacrifice. Dissected samples containing abutment, implant, and soft and hard tissues were obtained for histological processing. A, Group A (concave abutment); B, Group B (wider abutment).

surgeon. Each mandible containing the implants and hard and soft tissues was block-sectioned (Figure 2) and immersed in a fixative solution of 4% formalin. The fixed samples were dehydrated in a graded ethanol series using a dehydration system with agitation and a vacuum. The blocks were infiltrated with Technovit 7200® resin (Heraeus Kulzer, Hanau, Germany). The infiltrated specimens were placed into embedding molds, and polymerization was performed under ultraviolet light. The polymerized blocks were then sectioned in buccolingual direction, parallel to the long axis of each implant. Two slices were obtained per implant, and the slices were reduced by microgrinding and polishing using an Exakt grinding unit (Exakt, Norderstedt, Germany) to an even thickness of approximately 30 to 60 μm .

Sections were stained with Masson-Goldner trichrome as birefringence enhancement stain in order to facilitate measurement precision, whereby the staining enhanced the light intensity of the tissue samples under the polarized light microscope. This produced a clear image that permitted the accurate observation of collagen in various biological tissues.

Histomorphometric Circularly Polarized Light Assesment

Three expert pathologists were calibrated. Each one performed three repeated measurements of every variable. The data obtained were collated, and the intraclass correlation coefficient (ICC) was calculated with a value between 0.8 and 0.9, which was considered reliable.

As the subject of this study was supracrestal connective tissue (other longitudinal measurements such as biologic width, bone-to-implant contact, etc., were reserved for a future study with a different analytical approach), this was assessed by placing the stained sections under an Axiolab light microscope (Zeiss, Oberkochen, Germany), equipped with two linear polarizers and two quarter wave plates arranged to receive transmitted circularly polarized light. Collagen fibers aligned transversely to the direction of the light propagation (parallel to the plane of the section) appeared bright owing to a change in the refraction of the existing light, whereas the collagen fibers aligned along the axis of light propagation (perpendicular to the plane of the section) appeared dark because no refraction occurred.

Each slide was observed at magnifications of $\times 5$, $\times 10$, and $\times 20$, so that the field of analysis was located in the coronal third of the implant. The region of interest (ROI) was polygonal and contained all supracrestal connective tissue whose boundaries were medial (sulcular epithelium, healing abutment, or implant surface), lateral (vestibular gingival or vestibular lingual epithelium), coronal (coronal gingival epithelium), or basal (the most coronal portion of crestal bone) (Figure 3).

A grid of 8 mm length \times 8 mm width was superimposed on the image, with a total of 405 microareas of 100 μm \times 100 μm . The image was divided into vertical thirds (internal, medial, external) and horizontal thirds (coronal, medial, basal) of similar dimensions, making a total of nine coordinated areas – BI (basal-internal), BM (basal-medial), BE (basal-external), MI (medial-internal), MM (medial-medial), ME (medial-external), CI (coronal-internal), CM (coronal-medial), CE (coronal-external) – and thereby providing detailed information within the ROI. Each coordinate area contained 44 microareas (Figure 4).

Connective tissue contact (direct connection of connective tissue to healing abutment or implant surface) in three zones (BI, MI, and CI) was expressed in millimeters. Where there was no contact, the space between connective tissue and healing abutment or implant surface was measured and expressed in millimeters.

The connective tissue thickness (width of the connective tissue inside the ROI along three lines) was calculated as follows: after ROI selection, three areas were

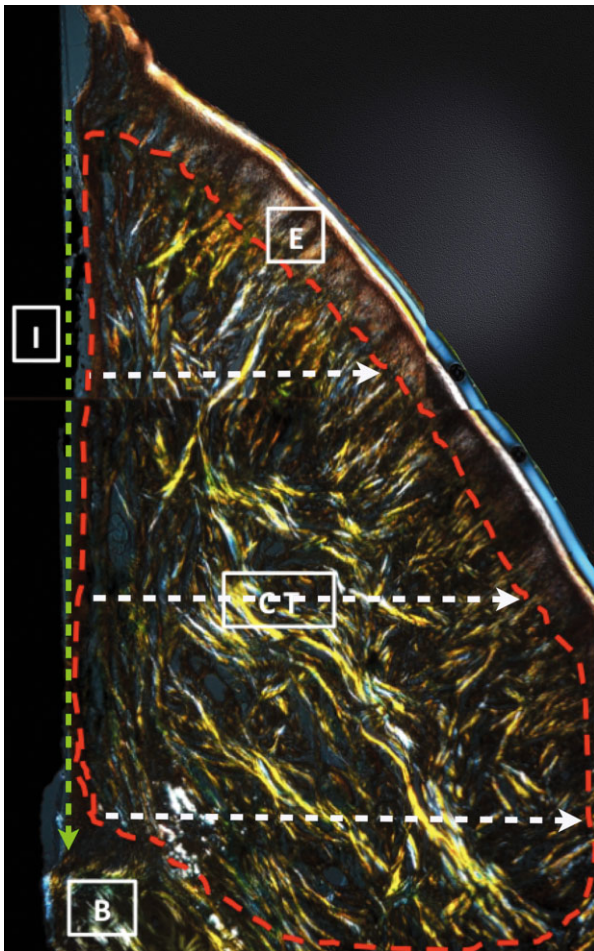


Figure 3 Region of interest. All supracrestal connective tissue (CT), delimited by the implant or abutment Surface to the inner aspect (I), by bone at the basal zone (B), and by the gingival epithelium to the external aspect (E). The green arrow shows the area selected for connective tissue contact evaluation; the white arrows show the areas where connective tissue thickness was evaluated.

measured – crestal, medial, and basal; three horizontal lines were drawn as an extension of the implant/abutment junction, in perpendicular direction from implant abutment to the epithelium (Figure 5). The length of each line was measured and registered; the mean thickness was calculated by averaging the three values, expressed in millimeters.

Fiber orientation within each microarea was determined in relation with the long axis of the implant using the ImageJ software angle measurement tool (U.S. National Institutes of Health, Bethesda, MD, USA) and registered manually, taking the position of the fibers from coronal to basal direction in a clockwise motion as reference, according to the scheme shown in Figure 6. Information on buccal and lingual sides was recorded in order to perform the measurements on the lingual side; using the same clockwise motion and coordinate areas, the images of the lingual side were rotated 180° in the horizontal direction to obtain a mirror image by means of image analysis software (ImageJ, U.S. National Institutes of Health).

If a microarea had two or more fiber orientations, the prevalent orientation was selected, resulting in a single value for each microarea. Fibers were considered parallel when they ran at angles of between 0° and 22.5° or between 155.5° and 180°; fibers were considered perpendicular at angles between 67.5° and 112.5°; fibers were considered oblique at angles between 22.5° and 67.5° and between 112.5° and 155.5° (Figure 6).

Fiber orientation in each coordinated area was expressed as a percentage, so that each coordinate area

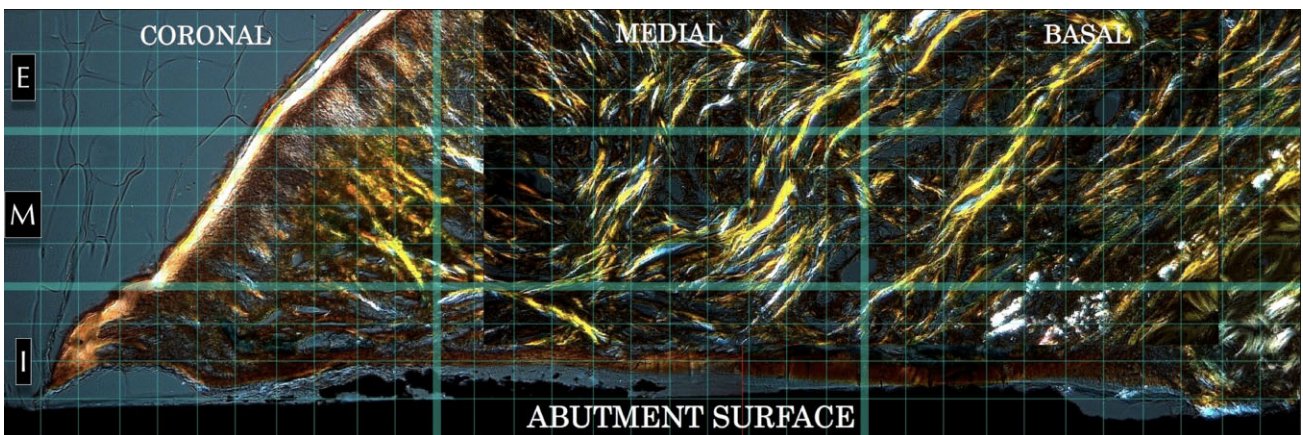


Figure 4 Coordinate areas or zones. A special grid of 405 microareas of 100 $\mu\text{m} \times 100 \mu\text{m}$ was superimposed over each slide. Three zones were evaluated in the horizontal direction: internal (I), medial (M), and external (E); three zones were evaluated in the vertical direction: coronal, medial, and basal. In this way, the coordinates map nine evaluation zones: coronal-internal, coronal-medial, coronal-external, medial-internal, medial-medial, medial-external, basal-internal, basal-medial, basal-external.

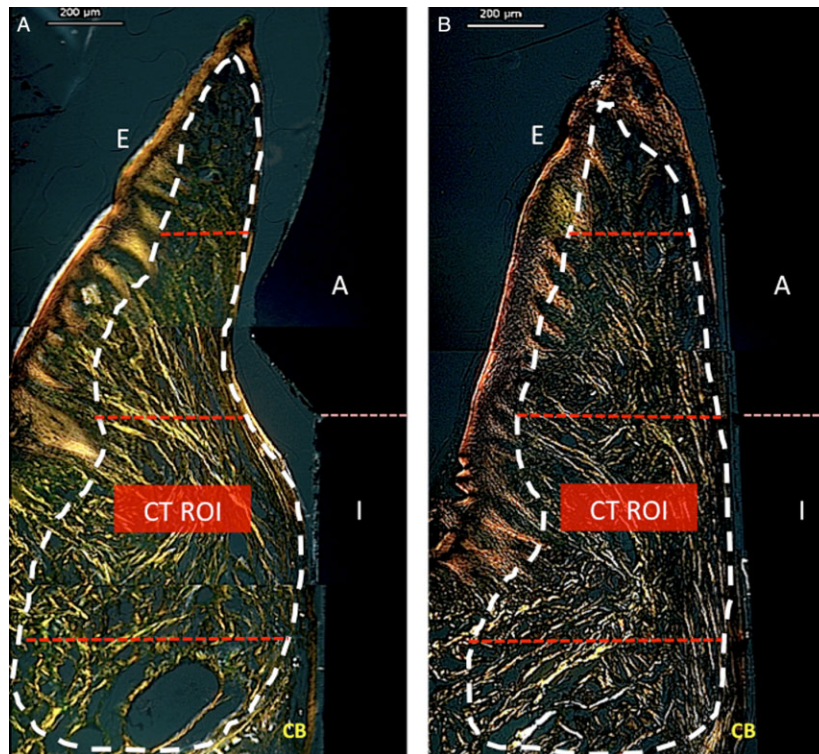


Figure 5 Connective tissue thickness. The connective tissue region of interest (CT ROI) is marked by white dots; red dotted lines show the three measurements taken for each abutment configuration. A, Group A; B, Group B. A = abutment; CB = crestal bone; E = epithelium; I = implant.

had 44 microareas adding up to 100%; the percentages were estimated by the following formula:

$$\text{Fiber orientation in coordinate area} = \text{number of areas with specific angle} \times 100/44.$$

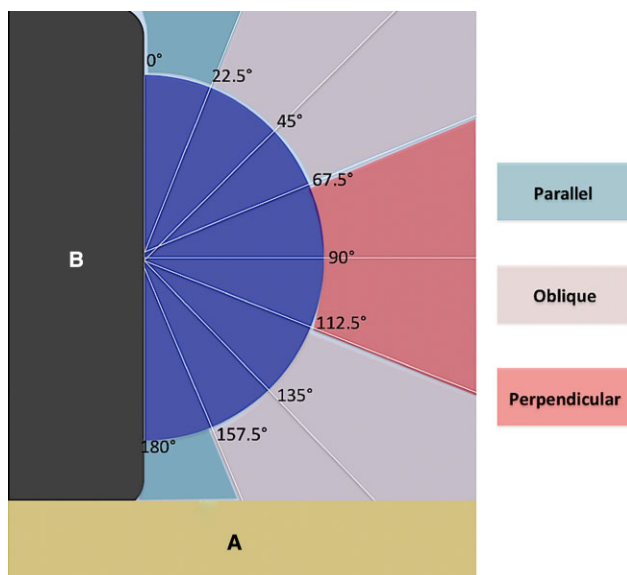


Figure 6 Collagen fiber orientation. A, Bone. B, Abutment/implant surface. Different orientations are marked with colors to facilitate observation.

Fiber density inside each ROI was expressed as a percentage, obtained by counting the number of fibers per microarea for each coordinate; each coordinate area had 44 microareas (100%), with fiber density calculated by the following formula:

$$\text{Fiber density in coordinate area} = \text{number of fibers in all microareas} \times 100/44.$$

Statistical Analysis

Intraobserver and interobserver reliability were analyzed using the ICC. A value between 0.8 and 0.9 was considered a positive correlation. Data were expressed as percentages, millimeters, and micrometers and mean and standard deviations.

The *t*-test was performed to detect differences in fiber orientation between different abutments. To confirm the results, a nonparametric, post hoc Wilcoxon ranked test was performed; *p* values < 0.05 were considered as significant.

RESULTS

ICC values were 0.9 for all three examiners and were considered reliable. After 3 months of healing, no

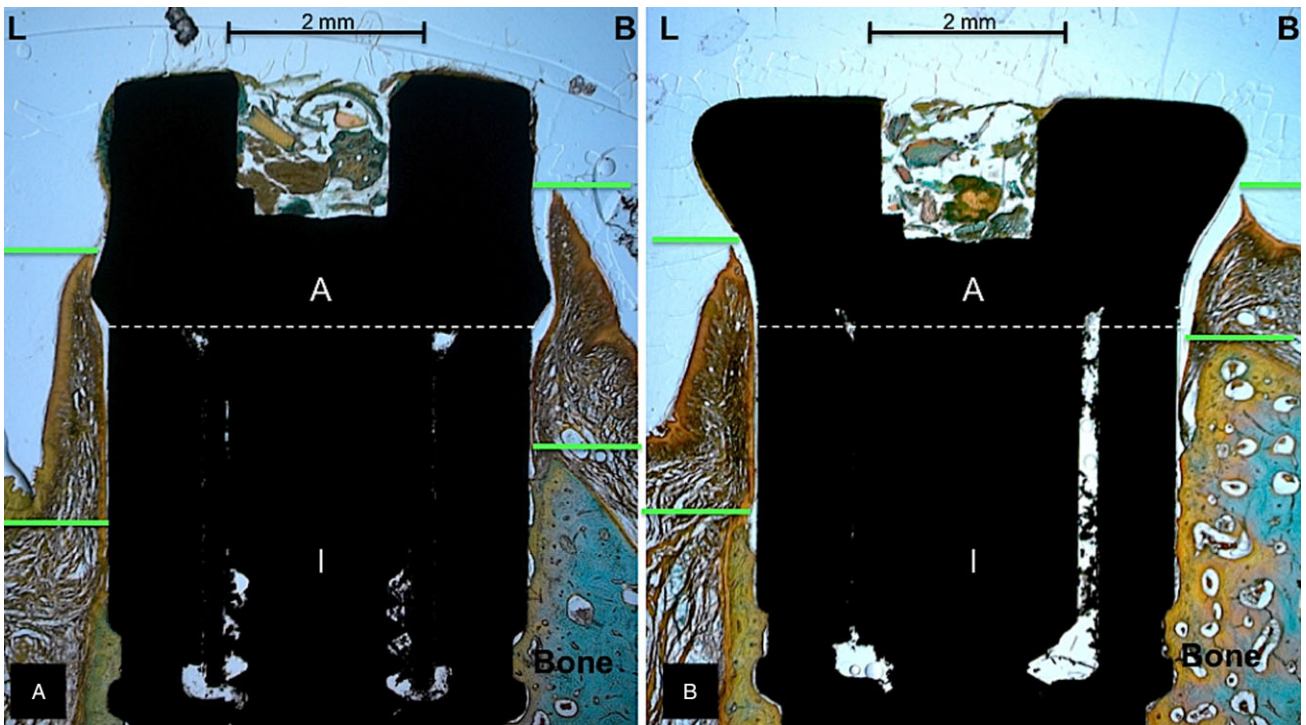


Figure 7 Histologic panoramic view of the two study groups. *A*, Concave abutment. *B*, Wider abutment. Green lines show the upper and lower soft tissue limits; white lines show the implant/abutment junction. A = abutment; B = buccal; I = implant; L = lingual.

implants or healing abutments had been lost or presented mobility, and no complications were observed during the healing period. Bleeding and gingival inflammation were not observed.

Histological Findings

No insertion or direct connective tissue contact with the abutment surfaces was observed in either study group. The spaces between abutments and soft tissues were similar in both groups. The basal area near to the bone was rich in blood vessels and less dense in fiber content, while connective tissue fibers were denser in the medial coordinates. Figure 7 shows a panoramic view of the samples stained with Masson-Goldner trichrome.

Connective Tissue Contact

Connective tissue contact with the abutment surface or with the implant surface was not observed in any case; instead, spaces were observed in all samples. These spaces were similar in both groups, without significant differences ($p > .05$). The coronal coordinate in both groups showed a larger mean space in comparison with the medial and basal coordinates (Table 1 and Figure 8).

Connective Tissue Thickness

The basal area showed significantly higher connective tissue thickness in both groups from $795 \pm 20 \mu\text{m}$

(Group A) to $810 \pm 10 \mu\text{m}$ (Group B) in comparison with the medial and coronal thirds ($p < .05$). The thickness of the medial third was slightly higher for Group B in comparison with Group A, without significant differences ($p > .05$). The coronal third showed the lowest thickness, without significant differences between groups ($p > .05$) (Table 2 and Figure 9).

Collagen Fiber Density

Basal. Fiber density in the BI zone was similar for both groups; in the BM zone, fiber density was greater in both groups in comparison with the basal and external zones; in the BE zone, fiber density was significantly higher in Group B ($p < .05$) (Table 3).

TABLE 1 Distance between Connective Tissue and Healing Abutment Surfaces (μm) ($n = 18$ per Group)

Surface	Group A (Concave)	Group B (Wider)
Basal-Internal	25 ± 0.7	24 ± 0.8
Medial-Internal	32 ± 0.4	30 ± 0.6
Coronal-Internal	$96 \pm 13^*$	$94 \pm 15^*$

Values expressed as mean \pm standard deviation.

The *t*-test showed more space in the coronal zone in comparison with the medial and basal zones in both groups.

* $p < .05$.

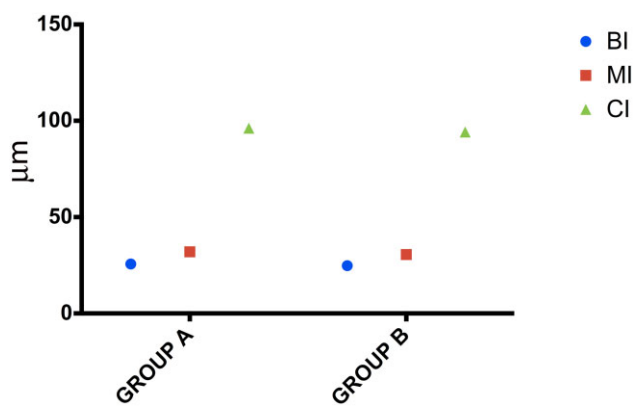


Figure 8 Connective tissue distance. The distance at coronal level was higher in both groups; in medial and basal zones, no differences were appreciated between groups. BI = basal-internal; CI = coronal-internal; MI = medial-internal.

Medial. Fiber density at the medial zone was higher in comparison with the basal zone. The MI zone showed no differences between groups. The MM zone showed the highest density of all zones, with significantly higher density in Group B ($p < .05$). The ME zone showed lower fiber density in comparison with the MM zone, but without differences between groups (Table 3).

Coronal. Fiber density in the coronal zone showed the lowest fiber density in comparison with the medial and

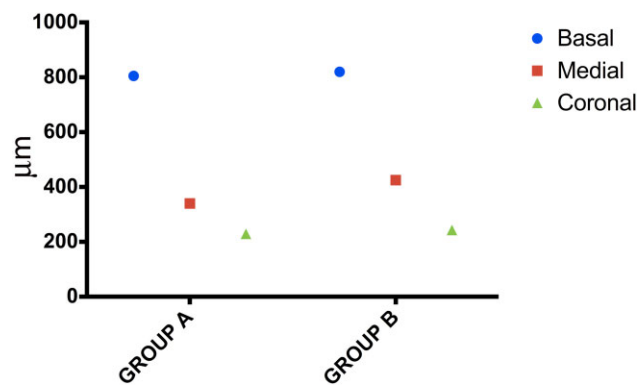


Figure 9 Connective tissue thickness. The basal zone showed greater thickness in both groups in comparison with the medial and coronal zones.

basal zones in both groups. The CI zone did not contain any fibers in either group. The CM zone and the CE zone showed similar fiber densities, without significant differences between the groups ($p > .05$) (Table 3).

Collagen Fiber Orientation

The fibers in the two groups showed different orientations. However, a common characteristic for both groups was that fibers entwined with other fibers in four different zones: at the union between external coordinates and medial coordinates, at the union between basal coordinates and medial coordinates, at the union between medial and internal coordinates, and inside the medial zone (Figure 10).

Basal. Mainly oblique fibers were observed in this area, beginning at the bone crest and running upward and inward; a small number of parallel fibers were also seen, without statistically significant differences between groups ($p < .05$). Some perpendicular fibers were found in the BE zones in both groups, which were significantly more numerous in Group B (38.3 ± 1.2) compared with Group A (26.5 ± 1.8) ($p < .05$) (Tables 4 and 5; Figure 11).

TABLE 2 Connective Tissue Thickness Measured along Three Lines in Connective Tissue inside the Region of Interest (µm) ($n = 18$ per Group)

Line	Group A (Concave)	Group B (Wider)
Basal	795 ± 10*	810 ± 10*
Medial	330 ± 10	410 ± 15
Coronal	224 ± 5	230 ± 13

Values expressed as mean ± standard deviation. The *t*-test showed greater thickness in the basal zone in both groups. * $p < .05$.

TABLE 3 Collagen Fiber Density (%)

	Basal			Medial			Coronal		
	Internal	Medial	External	Internal	Medial	External	Internal	Medial	External
Group A	11 ± 1.3	36.2 ± 4	17.26 ± 2.4	6.8 ± 1.2	68.18 ± 0.2*	34.09 ± 0.1	0.0	1.1 ± 0.2	0.8 ± 0.3
Group B	12 ± 1.1	72.75 ± 2.5*	20.21 ± 4.2	7.63 ± 0.5	81.81 ± 3.7*	54.15 ± 3.5*	0.0	1.2 ± 0.3	1.6 ± 0.4

Values expressed as mean ± standard deviation. * $p < .05$.

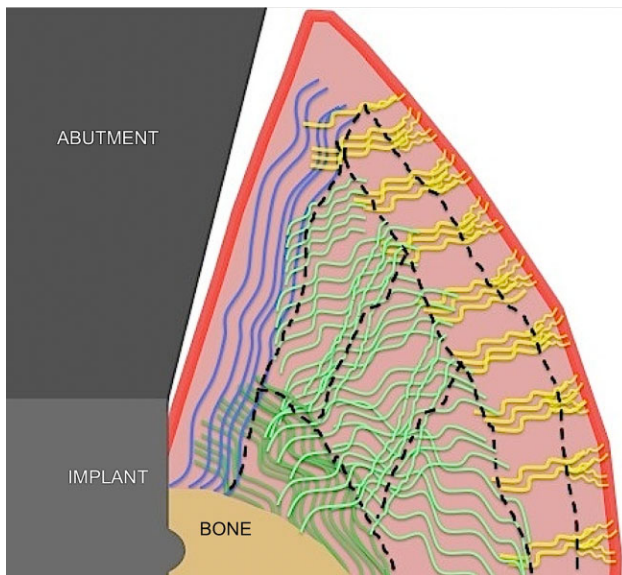


Figure 10 Crossing areas of collagen fibers. The black lines show the contact and crossing areas between fibers of different orientations. Four areas were detected: medial-external, medial-basal, medial, and medial-internal.

Medial. The medial zone showed a large number of fibers with different orientation. A significantly greater presence of perpendicular fibers was detected in the ME and MM zones in Group B compared with Group A ($p < .05$) (Tables 4 and 5; Figure 12).

Coronal. No significant differences were observed between groups at the coronal zones ($p > .05$). The CI area showed no fibers in either group. The CM zone showed mainly fibers of oblique orientation in both groups. The CE zone showed mainly perpendicular

fibers in both groups. At higher magnifications, the external zones in all groups showed microfibrer arrangements that originated at the epithelium, followed by bigger fibers running into the medial zone (Figure 13). The incorporation of a K2 filter in the polarizer facilitated the observation in increased detail of the microfibrers and the origins of collagen fibers of bigger size according to the different areas in the external zone (Figure 14).

DISCUSSION

The aims of the present work were to test if the geometry of healing abutments might modify connective tissue contact, thickness, density, and orientation characteristics and to validate the accuracy of a new method using coordinated microareas in an ROI that included all supracrestal connective tissue.

To date, most research has only considered vertical measurements related to the contact between connective tissue and the abutment/implant surface, so that other valuable information about supracrestal and transversal connective tissue has been ignored. In the present study, the inner border of the ROI was delimited by the abutment/implant surface and the outer by the gingival epithelium, and the border of the basal zone by the crestal bone.

To ensure the accuracy of the method, mean values were calculated using three repeated measurements, each performed by each of the three operators, and an ICC between operators was established. The ICC value obtained of 0.9 was considered reliable.

TABLE 4 Collagen Fiber Orientation in Group A (Concave) (%)

Zone	Parallel (0–22.5°)	Oblique (22.5–45°)	Oblique (45–67.5°)	Perpendicular (67.5–112.5°)	Oblique (112.5–135°)	Oblique (135–155.5°)	Parallel (155.5–180°)
Basal-internal	–	3.1 ± 0.4	–	–	28.3 ± 0.2	27.9 ± 0.2	–
Basal-medial	5.8 ± 0.8	–	–	–	27.6 ± 1.5	12.8 ± 0.2	30.1 ± 1.4
Basal-external	–	–	–	26.5 ± 1.8	18.3 ± 0.8	–	–
Medial-internal	–	–	8.3 ± 1.4	–	16.2 ± 2.1	–	–
Medial-medial	7.5 ± 0.2	11.2 ± 0.8	12.2 ± 1.8	3.6 ± 0.4	10.8 ± 1.9	23.4 ± 1.5	5.1 ± 0.8
Medial-external	–	–	–	26.2 ± 1.6	–	–	2.7 ± 0.4
Coronal-internal	1.2 ± 0.6	–	–	–	–	–	–
Coronal-medial	–	–	–	–	–	2.3 ± 0.6	–
Coronal-external	–	–	–	25.2 ± 3.7	–	–	–

Values expressed as mean ± standard deviation.

* $p < .05$.

TABLE 5 Collagen Fiber Orientation in Group B (Wider) (%)

Zone	Parallel (0–22.5°)	Oblique (22.5–45°)	Oblique (45–67.5°)	Perpendicular (67.5–112.5°)	Oblique (112.5–135°)	Oblique (135–155.5°)	Parallel (155.5–180°)
Basal-internal	0.8 ± 0.5	2.1 ± 0.3	–	–	23.1 ± 0.3	38.3 ± 0.7	–
Basal-medial	–	–	–	–	17.6 ± 1.5	16.6 ± 0.09	25.3 ± 1.8
Basal-external	–	–	–	38.3 ± 1.2	19.2 ± 0.8	–	–
Medial-internal	–	–	14.2 ± 1.8	13.4 ± 0.9	13.4 ± 1.5	–	–
Medial-medial	1.3 ± 0.2	17.2 ± 1.4	32.2 ± 1.8	9.6 ± 0.8	10.8 ± 1.9	28.7 ± 1.3	5.3 ± 0.2
Medial-external	–	–	–	39.3 ± 1.4	–	4.1 ± 0.3	3.1 ± 0.5
Coronal-internal	1.4 ± 0.3	–	–	–	–	–	–
Coronal-medial	–	–	–	–	–	–	–
Coronal-external	–	–	9.1 ± 0.6	26.6 ± 2.4	–	–	–

Values expressed as mean ± standard deviation.

* $p < .05$.

Regarding connective tissue contact with the healing abutment surfaces, no contact was observed in either of the study groups. The absence of contact might be explained by two factors: sample processing and the abutment surfaces, which were of minimal roughness (R_a $0.3 \mu\text{m} \pm 0.1 \mu\text{m}$). This concurs with research carried out by Nevins and colleagues,^{18,19} Pecora and colleagues,²⁰ and Zhao and colleagues,²¹ who showed that some types of special surface topography such as microgrooves or micropits are needed to achieve contact and the insertion of connective tissue fibers into the abutment/implant surface.

Given that two healing abutment designs of different geometry were tested in the study, it was expected that connective tissue would vary according to the

abutment type, and this proved to be the case. The thinnest part of the connective tissue corresponded to the coronal third in both groups. However, in the middle part, differences in thickness were observed, thickness being less in the medial area of Group A abutments and thicker in the medial section of Group B abutments.

Perhaps the presence of a convex area in the Group A abutments resulted in thinning due to compression of the connective tissue, while the wide Group B abutments resulted in a thickening towards the medial zone due to a displacement of connective tissue.

The authors have been unable to locate any published research in the literature that might explain the differences in connective tissue thickness resulting from abutment geometry.

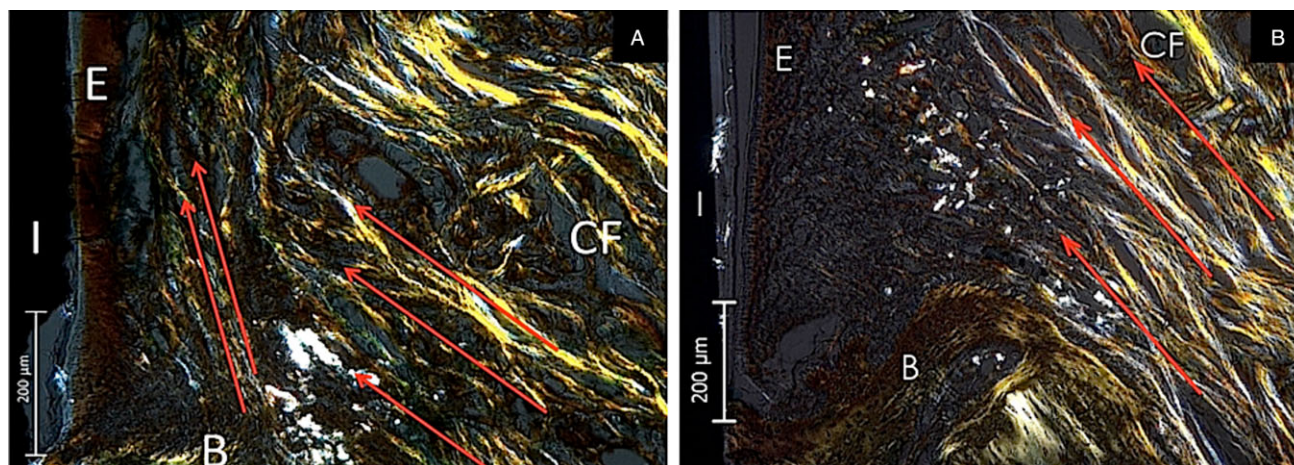


Figure 11 Collagen fiber orientation at basal zone. The fibers follow an oblique orientation in both groups, with some parallel fibers in group A. A, Group A. B, Group B. B = bone; CF = connective fibers; E = epithelium; I = implant.

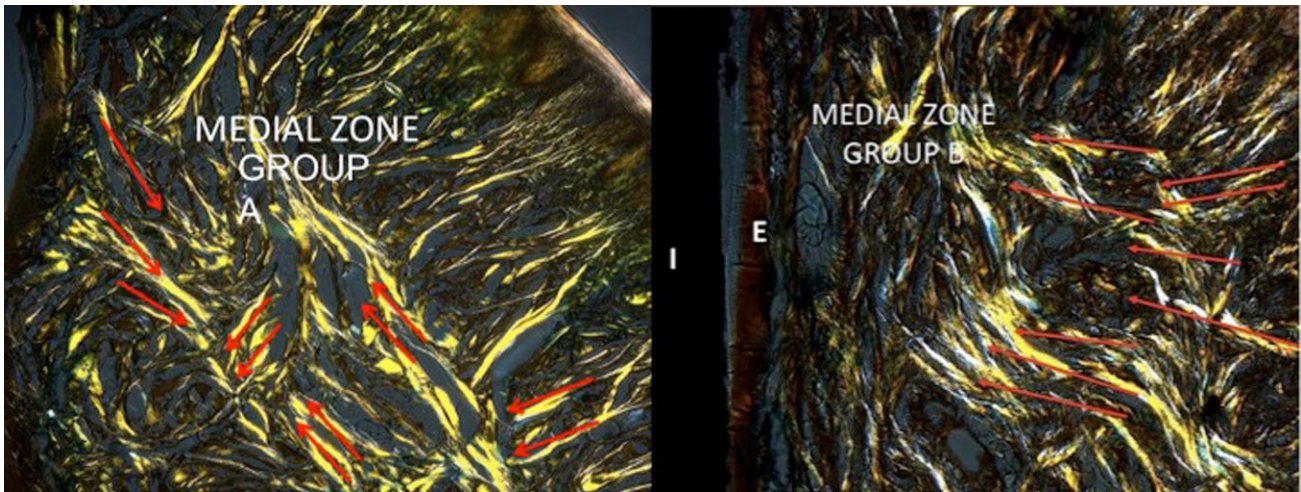


Figure 12 Collagen fiber orientation at medial zone. The medial zone presents a mixed fiber orientation, with the predominant presence of oblique fibers in group A (left) and perpendicular fibers in group B (right). E = epithelium; I = implant.

However, it is understood that connective tissue forms a protective web around the implant or abutment collar, and it can be expected that the greater the thickness of connective tissue, the greater resistance to the mechanical forces arising from mastication.^{27,28} The present study did not take initial measurements of the connective tissue thickness before the study procedures commenced. However, the differences found between groups in single dogs justify the effect of healing abutment geometry on tissue thickness.

The study of collagen fiber density identified which zones presented the highest numbers of fibers within the total supracrestal connective tissue thickness. This is the first time that this factor has been studied in relation to healing abutment shape. It was found that the basal (BM, BE) and medial (MM, ME) zones in both groups showed greater fiber density, while the internal zones (BI, MI, CI) lacked fibers.

The higher density of fibers in the basal and medial zones in both groups could be due to the thickness of connective tissue in the basal area or the origin of the fibers in the periosteum of the cortical bone, from which they spread toward the medial zone. The higher density

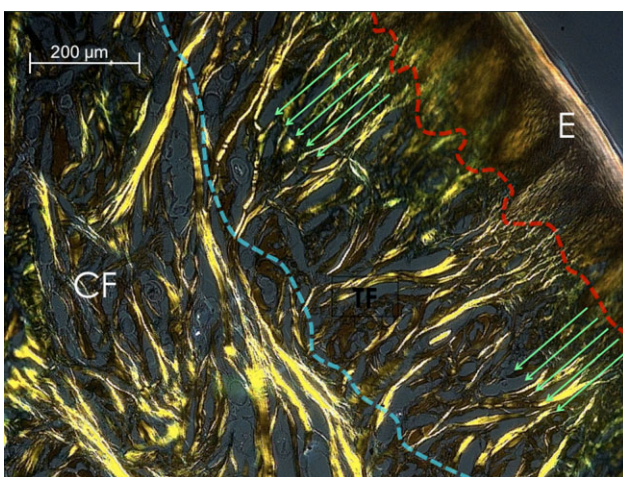


Figure 13 Collagen fiber orientation in external zone (detail). The epithelium is the source of microfibrils that form bundles; these bundles form bigger fibers connecting the epithelium to the medial zone. CF = collagen fibers; E = epithelium; TF = transverse fibers. The red dotted line is showing the external epithelium zone. The blue dotted line is showing the transition between the external zone and the medial zone.

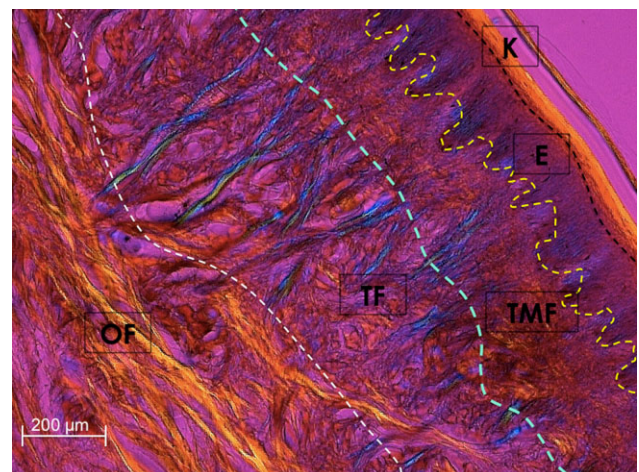


Figure 14 Collagen fiber orientation in external zone (processed image). The incorporation of a K2 filter provides a better image of the origin of epithelial connective fibers. E = epithelium; K = external epithelium; OF = oblique fibers; TF = transverse fibers; TMF = transverse microfibrils.

of fibers in the basal-external zone and medial-external zone could be due to the convergence of various groups of fibers, which join the gingival epithelium to connective tissue, forming a reinforcing structure around the healing abutments.

In order to study connective tissue fiber orientation, the long axis of the implant was used as reference, starting in the coronal zone and ending in the basal zone; fiber orientation was registered as forming a plane of between 0° and 180°, examining fiber orientation in 405 microareas of 100 µm × 100 µm. Data were classified as belonging to one of three groups: parallel fibers (fibers running at angles of between 0° and 22.5° or between 157.5° and 180°), oblique fibers (22.5° to 67.5° and 112.5° to 157.5°), and perpendicular fibers (67.5° to 112.5°).

No differences were found in connective tissue fiber orientation in relation to healing abutment geometry in the basal zone (BM, BE) or in the medial zone (MM, ME); although there was a slight predominance of parallel fibers in Group A compared with Group B in the MM zone, this difference was not significant ($p > .05$).

Previous studies by Comut and colleagues¹⁷ analyzed collagen fiber orientation in contact with implants in a region that varied from 0° to 90°, using hematoxylin and eosin stain, examining the samples with circularly polarized light. However, the narrow range of orientations considered excluded some orientations occurring in supracrestal connective tissue.

A recent pig study by Tete and colleagues²⁹ used the same criteria as Comut and colleagues; when fiber orientations around titanium and zirconia implants were compared, it was found that fiber orientation was mainly parallel and oblique in both groups. This coincides with the present study, which identified a predominance of oblique and parallel fibers in zones MB and MM in Group A and a predominance of oblique fibers in Group B.

Rodríguez and colleagues³⁰ studied collagen fiber orientation and bone resorption around implants in relation to the platform-switching technique; after various manipulations of abutments with platform switching versus abutments with standard platforms, it was found that fibers established contact at the level of the platform for the implants that underwent platform switching and at the level of the first spiral thread for standard implants.

The presence of a group of circular fibers described by Rodríguez and colleagues³⁰ is similar to the findings of the present study for zones MB and MM. However, the authors do not describe the method used to determine fiber orientation, a further difference between their study and the present work, which found another band of perpendicular fibers connecting the epithelium with the connective tissue in the BE and ME zones.

Zhao and colleagues²¹ studied implants that had been modified at the neck to create pits of different sizes, comparing these with implants without pits. It was found that with the presence of surface pits, fibers aligned obliquely and perpendicularly, as the fibers were able to anchor themselves, in contrast to the implants without modification, where the fiber orientation was mainly parallel.

This coincides with the present study in that the surfaces of the abutments or their necks did not undergo modification, which resulted in parallel fiber orientation in all internal zones (BI, MI, CI) and an absence of contact with the abutment surfaces.

Collagen fibers around healing abutments of different geometry produced similar results in the internal basal zone (BI) and the external zone (BE, ME) but produced differences in all the medial zones, where Group A abutment geometry exercised some influence, resulting in mainly oblique fiber orientation. The explanation of fiber orientation remains unclear, although two possible factors have been described whereby, firstly, during the healing process the flux of fibroblasts will reorganize the collagen fibers and, secondly, collagen will align with tension lines in response to large tissue displacements.³¹

The present study set out to provide additional information about supracrestal connective tissue by describing in detail and applying a research method that can be reproduced. Although this has generated new information, the data should be treated with caution in the light of several factors: the small size of the sample; the thickness of the histological sections, which could have affected the interpretation of fiber density and orientation; the lack of attachment between connective tissue and abutment/implant surface, which may have influenced the orientation of fibers; and the staining procedure, which, although it facilitated fiber observation, depends on the direction of histological sectioning.

The clinical implications of this study address the choice of healing abutments, whereby an abutment of a wide profile will favor connective tissue of greater thickness and oblique and perpendicular fiber orientation, as well as better performance when subjected to the mechanical forces generated by mastication and the prevention of apical migration of junctional epithelium. While a concave abutment will result in less connective tissue thickness and oblique fiber orientation without perpendicular fibers, this will result in less opposition to apical migration of connective tissue and lower resistance to mechanical mastication forces.

The results need to be confirmed through analysis of more healing abutment geometries, using the method described above.

CONCLUSIONS

Within the limitations of the present study, it may be concluded that an abutment of larger coronal diameter than the implant platform favors oblique and perpendicular collagen fiber orientation and greater connective tissue thickness.

REFERENCES

1. Siar CH, Toh CG, Romanos G, et al. Periimplant soft tissue integration of immediately loaded implants in the posterior macaque mandible: a histomorphometric study. *J Periodontol* 2003; 74:571–578.
2. Schierano G, Ramieri G, Cortese MG, Aimetti M, Preti G. Organization of the connective tissue barrier around long-term loaded implant abutments in man. *Clin Oral Implants Res* 2002; 13:460–464.
3. Listgarten MA, Lang NP, Schroeder HE, Schroeder A. Periodontal tissues and their counterparts around endosseous implants. *Clin Oral Implants Res* 1991; 3:1–19.
4. Ericsson I, Persson LG, Berglundh T, Marinello CP, Lindhe J, Klinge B. Different types of inflammatory reactions in periimplant soft tissues. *J Clin Periodontol* 1995; 22:255–261.
5. Abrahamsson I, Berglundh T, Lindhe J. Soft tissue response to plaque formation at different systems. A comparative study in the dog. *Clin Oral Implants Res* 1998; 9:73–79.
6. Hermann JS, Buser D, Schenk RK, Higginbottom FL, Cochran DL. Biologic width around titanium implants. A physiologically formed and stable dimension over time. *Clin Oral Implants Res* 2000; 11:1–11.
7. Hansson S. The dental implant meets bone: a clash of two paradigms. *Appl Osseointegration Res* 2006; 5:5–17.
8. Berglundh T, Lindhe J, Ericsson I, Marinello CP, Liljenberg B, Thomsen P. The soft tissue barrier at implants and teeth. *Clin Oral Implants Res* 1991; 2:81–90.
9. Buser D, Weber HP, Donath K, Fiorellini JP, Paquette DW, Williams RC. Soft tissue reactions to non-submerged unloaded titanium implants in beagle dogs. *J Periodontol* 1992; 63:225–235.
10. Abrahamsson I, Berglundh T, Lindhe J. Soft tissue response to plaque formation at different implant systems. A comparative study in the dog. *Clin Oral Implants Res* 1998; 9:73–79.
11. Glauser R, Schupbach P, Gottlow J, Hämmerle CHF. Peri-implant soft tissue barrier at experimental one-piece mini-implants with different surface topography in humans: a light-microscopic overview and histometric analysis. *Clin Implant Dent Relat Res* 2005; 7(S1):S44–S51.
12. Ten Cate AR. The role of epithelium in the development, structure and function of the tissues of tooth support. *Oral Dis* 1996; 2:55–62.
13. Schroeder HE, Listgarten MA. The gingival tissues: the architecture of periodontal protection. *Periodontol* 2000 1997; 13:91–120.
14. Bosshardt DD, Lang NP. The junctional epithelium: from health to disease. *J Dent Res* 2005; 84:9–20.
15. Schupbach P, Glauser R. The defense architecture of the human periimplant mucosa: a histological study. *J Prosthet Dent* 2007; 97:S15–S25.
16. Schupbach P, Hurzeler M, Grunder U. Implant-tissue interfaces following treatment of peri-implantitis using guided tissue regeneration: a light and electron microscopic study. *Clin Oral Implants Res* 1994; 5:55–65.
17. Comut AA, Weber HP, Shortkroff S, Cui FZ, Spector M. Connective tissue orientation around dental implants in a canine model. *Clin Oral Implants Res* 2001; 12:433–440.
18. Nevins M, Nevins ML, Camelo M, Boyesen JL, Kim DM. Human histologic evidence of a connective tissue attachment to a dental implant. *Int J Periodontics Restorative Dent* 2008; 28:111–121.
19. Nevins M, Kim DM, Jun SH, Guze K, Schupbach P, Nevins ML. Histologic evidence of a connective tissue attachment to laser microgrooved abutments: a canine study. *Int J Periodontics Restorative Dent* 2010; 30:245–255.
20. Pecora GE, Ceccarelli R, Bonelli M, Alexander H, Ricci JL. Clinical evaluation of laser microtexturing for soft tissue and bone attachment to dental implants. *Implant Dent* 2009; 18:57–66.
21. Zhao BH, Han H, Feng HL, Bai W, Cui FZ, Lee IS. Histomorphometrical and clinical study of connective tissue around titanium dental implants with porous surfaces in a canine model. *J Biomater Appl* 2013; 27:685–693.
22. Rompen E, Raepsaet N, Domken O, Touati B, Dooren E. Soft tissue stability at the facial aspect of gingivally converging

- abutments in the esthetic zone: a pilot clinical study. *Journal of Prosthetic Dentistry* 2007; 97:119–125.
23. Patil R, van Brakel R, Iyer K, Huddleston Slater J, de Putter C, Cune M. A comparative study to evaluate the effect of two different abutment designs on soft tissue healing and stability of mucosal margins. *Clin Oral Implants Res* 2013; 24: 336–341.
 24. Welander M, Lekovic V, Spadijer-Gostovic S, Milicic B, Wegscheider W, Piehlsinger E. Soft tissue development around abutments with a circular macro-groove in healed sites of partially edentulous posterior maxillae and mandibles: a clinical pilot study. *Clin Oral Implants Res* 2010; 22:743–752.
 25. Welander M, Abrahamsson I, Berglundh T. The mucosal barrier at implant abutments of different materials. *Clin. Oral Impl Res* 2008; 19:635–641.
 26. Myshin HL, Wiens JP. Factors affecting soft tissue around dental implants: a review of the literature. *J Prosthet Dent* 2005; 94:440–444.
 27. Schnitz N, Laverty S, Kraus VB, Aigner T. Basic methods in histopathology of joint tissues. *Osteoarthritis Cartilage* 2010; 18:113–116.
 28. Goktas S, Dmytryk J, McPettridge S. Biomechanical behavior of oral soft tissues. *J Periodontol* 2011; 82:1178–1186.
 29. Tete S, Mastrangelo F, Bianchi A, Zizzari V, Scarano A. Collagen fiber orientation around machined titanium and zirconia dental implant necks: an animal study. *Int J Oral Maxillofac Implants* 2009; 24:52–58.
 30. Rodriguez X, Vela X, Calvo-Guirado J, Nart J, Stappert F. Effect of platform switching on collagen fiber orientation and bone resorption around dental implants: a preliminary histologic Animal Study. *Int J Oral Maxillofac Implants* 2012; 27:1116–1122.
 31. Yang L, Witten TM. A biomechanical model of wound contraction and scar formation. *J Theor Biol* 2013; 332:228–248.

Copyright of Clinical Implant Dentistry & Related Research is the property of Wiley-Blackwell and its content may not be copied or emailed to multiple sites or posted to a listserv without the copyright holder's express written permission. However, users may print, download, or email articles for individual use.